Sensing and Bio-Sensing Research 32 (2021) 100414

Contents lists available at ScienceDirect

Sensing and Bio-Sensing Research

journal homepage: www.elsevier.com/locate/sbsr

Numerical investigation of the refractive index sensitivity of Au/Ag core-shell nanostructures for sensing applications

Géza Szántó [a,*], István Csarnovics [a], Attila Bonyár [b]

[a] Department of Experimental Physics, Institute of Physics, Faculty of Science and Technology, University of Debrecen, Debrecen, Hungary
[b] Department of Electronics Technology, Budapest University of Technology and Economics, Budapest, Hungary

ARTICLE INFO

Keywords:
Plasmonics
Core-shell bimetallic nanoparticle
Refractive index sensitivity
Localized surface plasmon resonance
Boundary element method

ABSTRACT

The plasmonic properties of bimetallic (gold and silver) core-shell nanostructures were studied numerically by using the boundary element method implemented in MATLAB (MNPBEM toolbox). The dependence of the bulk refractive index sensitivity of the nanostructures on the core/shell thicknesses was investigated, and regions of enhanced sensitivities were identified for both Ag@Au and Au@Ag type of nanostructures. For Ag@Au nanoparticles, utilizing a 14 ± 2 nm silver core radius with 4 ± 2 nm gold shell thickness or a 22 ± 2 nm core radius with 6 ± 1 nm shell thickness can yield a 1.2–2.5× increase in sensitivity compared to a purely silver nanosphere with the same size. For Au@Ag structures, 20 ± 3 nm gold core size with 10 ± 3 nm silver shell thickness was found to be optimal, with sensitivity enhancements between 2 and 5× compared to pure gold nanoparticles with the same size. The increased sensitivity can always be attributed to the hybridization of the plasmon absorbance peaks corresponding to the silver and gold parts, which merging comes with increased peak width (and thus decreased figure of merit) as a tradeoff. The provided sensitivity maps can be helpful for the design and fabrication of plasmonic sensors utilizing core-shell nanostructures.

1. Introduction

Localized surface plasmon resonance (LSPR) is the coherent oscillation of conduction electrons on a nanoparticle, incited by an electromagnetic wave. Since this oscillation frequency depends on the dielectric properties of the medium surrounding the nanoparticles, this phenomenon can be effectively utilized for sensing purposes in chemical and biosensors [1,2]. LSPR based refractive index (RI) sensing can be advantageous compared to the classical thin-film based Kretschmann SPR configurations since LSPR can be excited conveniently (without the use of a prism or adjusting angles), which would enable its integration into small diagnostic devices [3].

Since the RI sensitivity of an LSPR sensor is determined by the material composition, size, shape, and arrangement (i.e., interparticle gap) of the used nanoparticles [4], a large variety of diverse shapes and configurations are being tested for sensing, including nanoislands [5], nanodiscs [6], nanotriangles [7], nanocones [8], nanorings [9], or complex composite structures [10,11]. Bimetallic core-shell structures (mostly made from gold and silver) are also widely used for LSPR and also for SERS (surface-enhanced Raman spectroscopy) since their optical properties can be tuned by varying the core and shell thicknesses, as demonstrated with multiple methods [12–16]. Although the literature on Ag@Au and Au@Ag core-shell systems is extensive in terms of synthesis and optical properties, only a few groups investigated the refractive index sensitivity of these structures, e.g., Ag@Au [17,18], Au@Ag [19]. Since the optical properties and RI sensitivity both depend on the core/shell thicknesses of these structures, their optimization would be of great importance, considering sensing applications.

The change in the effective refractive index of the medium surrounding the nanoparticles is usually monitored through the shift of the peak in the wavelength-dependent optical cross-sections. Experimentally, the extinction cross-section is the easiest to measure from a directly transmitted beam, because it is the sum of the scattering and absorption cross-sections [20]. However, the optical description of core-shell structures is not as simple as a particle made of a single material. Hybridization theory allows the analysis of a more complex system by examining its components, so it could be suitable for the approximate characterization of the behavior of core-shell systems [21]. More accurate results can be obtained analytically by using the generalized Mie theory, however, this method cannot be applied to general forms and arrangements [22].

The optical properties of complex nanoshapes and arrangements can

* Corresponding author.
E-mail address: szanto.geza@science.unideb.hu (G. Szántó).

https://doi.org/10.1016/j.sbsr.2021.100414
Received 18 January 2021; Received in revised form 12 March 2021; Accepted 22 March 2021
Available online 23 March 2021

be investigated with the help of different numerical simulation approaches, such as DDA (discrete dipole approximation), FDTD (finite difference in the time domain), or finite element (FEM) based methods. In this work, the boundary element method (BEM) was used, which belongs to the class of finite element methods [23]. Its unique feature is that only the surface of the particle has to be discretized, so it is less computationally intensive compared to DDA, FDTD, or other FEM approaches [24].

This paper aims to utilize BEM simulations for the investigation of bimetallic Au/Ag core-shell nanostructures. Our main objective is the optimization of core/shell thicknesses for maximum refractive index sensitivities. This information can be used for the optimized design and fabrication of LSPR transducers utilizing such core-shell nanostructures.

2. Methods

For the simulations, the MNPBEM MATLAB toolbox was used [23], which was developed specifically for the simulation of nanoparticles and utilizes the boundary element method. From the simulation options, the 'ret' (retarded) solver was selected, which solves the complete Maxwell equations. The toolbox solves the BEM equations after specifying the excitation, and the arrangement, consisting of the particle and the surrounding dielectric. It calculates the charges and currents appearing inside and outside the particle interfaces so that the values of the electromagnetic fields can be calculated anywhere [23,25]. The extinction cross-section, calculated in the forward direction and assuming a small detector away from the particle, can then be queried with a single command. This is calculated using the optical theorem, which establishes a relationship between the extinction and the imaginary part of the scattering amplitude of the particle in the forward direction [26].

For the characterization of particles with different arrangements, the bulk refractive index sensitivity (RIS) was used, which is from now on referred to as sensitivity. Sensitivity can be calculated from the shifts of the peak observed at the extinction cross-sections of particles in two homogeneous media with different refractive indices. Measuring or computing bulk refractive index sensitivity (as defined by Eq. 1) is a commonly used simplification when characterizing plasmonic nanosensors [27]:

$$S = \frac{\lambda_2 - \lambda_1}{n_2 - n_1} = \frac{\Delta\lambda}{\Delta n} \tag{1}$$

Where λ_m is the wavelength of the peak in media m; n_m is the refractive index of media m, $n_2 > n_1$. Refractive indices were used in dimensionless [RIU].

The definition of sensitivity does not take into account that the broadening of the peaks impairs the perceptibility of the displacement during a measurement.

This problem can be considered by using the figure of merit (FOM), which is obtained by dividing the sensitivity by the full width at half maximum (FWHM) of the peak measured in [nm] [28], which is shown in Eq. 2:

$$FOM = \frac{S}{FWHM} \tag{2}$$

For our calculations, the FWHMs were approximated by the peak widths at half prominence, by using built-in MATLAB functions.

2.1. Simulation parameters

The size range to determine the RIS of pure gold and silver NPs was selected with based on the following considerations: There should be at least one definite peak in the visible spectrum, possibly in the near UV. Preliminary simulations showed that a few nm shell could have a significant effect, but in the case of 1 nm we experienced artifacts, which was no longer present at $r_s = 2nm$, so we chose this as the minimum layer thickness. The upper limit of the sizes is given by the peak at the small wavelength of the quadrupole mode for silver particles, which is difficult to ignore in the case of $r \gg 40nm$, but to discuss it would complicate the description without any added value, so we maximized the external size of the particles in $r_{\text{full}} = 43nm$. So the shell radius (r_{shell}) of the simulated nanoparticles were between $2nm$ and $38nm$, while the minimal inner core radius (r_{core}) was $5nm$. The full radius ($r_{full} = r_{core} + r_{shell}$) of the largest investigated particle was 43 nm. The resolution of the internal radius and the thickness of the shell was 1 nm. The surfaces of both the inner and the outer sphere were approximated by uniform triangulation by using 256 vertices, which was achieved via the 'trisphere' function of the MNPBEM toolbox. For comparison with the core-shell NPs' pure (single metal) spheres, nanoparticles built from 256 vertices were also used. A created model of a core-shell structure is illustrated in Fig. 1.

The frequency-dependent permittivity of gold and silver are required input parameters to perform the simulation. All the simulations were based on the measurement results of Johnson and Christy [29].

Plane-wave excitation was used with light propagation in the Z direction and light polarization in the X-direction.

Refractive indices $n_1 = 1.33$ RIU and $n_2 = 1.35$ RIU were selected to calculate the sensitivity. The $n = 1.33$ was chosen because chemical and biosensors mainly operate in aqueous media. Although the peaks' shift depends approximately linearly on Δn over a wide range [30], the used Δn value for the simulations should be selected carefully. A too-large Δn could make the related extinction peaks hard to identify and pair because of the complex spectra and interactions of core-shell systems. A too-small Δn would also not be advantageous, as it could amplify the numeric errors in the results. Our refractive indices were selected according to these considerations.

The location of the peaks was determined as follows: first, the local maxima of the extinction cross-section with a wavelength resolution of nm were determined, and then the position was further refined using the ± 3 nm environment of the local maximum. The precise determination of the position of the peak was achieved by fitting a second-degree polynomial to these points, which is a good approximation in such a small environment of the local maximum. The value where the derivative of the fitted function is 0 was used as the position of the peak. This method gives a more accurate position value than the local maxima found in the raw data, and the result of the fitting in a small environment of the local maxima corresponds to the results obtained by fitting the Gaussian function to the same data, but it can be performed much faster. Sensitivities were calculated from the defined ($n_1 = 1.33$ RIU, $n_2 = 1.35$ RIU) peak pairs using the formula already described in Eq. (1).

3. Results

It is widely known that the extinction spectra of geometrically

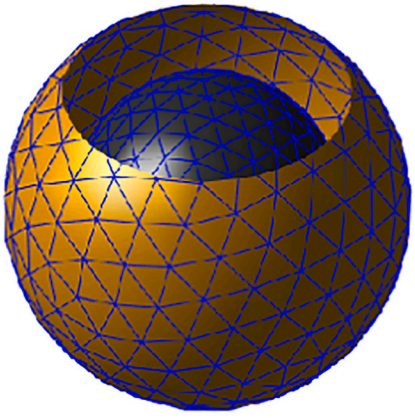

Fig. 1. Example of an Ag@Au core-shell nanosphere with the used 256 vertices resolution (the shell is cut out to reveal the core).

identical gold and silver nanoparticles are very different [31]. In the size range of 20 nm to 100 nm, the extinction peaks of silver particles in an aqueous medium are observed between 400 and 520 nm, while in the case of gold, between 525 and 580 nm [32]. An important difference is that the maximum extinction achievable with silver is more than an order of magnitude higher, moreover, its refractive index sensitivity is also much better than gold [28]. In the case of core-shell particles, the properties of both metals can be observed. As it could be expected, in the case of a thick shell, the properties of the outer metal dominate, while in the case of a thin shell, the properties of the core are more visible. However, the detailed description of the core-shell structure's behavior is more complex. Following the hybridization theory, in some cases, in addition to the peaks of the mere core and the mere shell, new hybrid peaks appear [33]. Thus, sensitivity calculations were performed separately for each peak, but only the dominant peak of the spectrum will be shown in the next figures.

3.1. The sensitivity of Ag@Au core-shell nanostructures

In the case of Ag@Au core-shell nanoparticles, (silver core and gold shell) two different types of peaks play a dominant role in the spectrum of the extinction cross-section, one peak belonging to the silver core while the other to the gold shell. The former is primarily present for thicker, while the latter is for thinner gold shells ($r_{shell} < 12\ nm$), but in some cases, the two types may be present simultaneously. Identification of the peaks' type was based on the wavelength of the peaks. As a rule of thumb, within the studied size range, peaks below 500 *nm* belong to the silver core, and all above belong to the gold shell. The range of different peaks can be illustrated well by displaying the wavelength of the highest peak, as illustrated in Fig. 2.

This approach is practical because further than 2 nm in any direction from the boundary, the secondary peaks are only marginal in height. The dominance transition of the primary peak was marked with a red line in Fig. 2.

If the gold shell is thin $(2-3)\ nm$, only the peak belonging to the silver core appears. The peak is well defined, they are also similar but wider than if the particles were made of only pure silver. In the case of a thicker $(4-10)\ nm$ gold layer, the peak of the shell also appears on the spectrum. The peak belonging to the core is broadened, not well defined, however, in this case, the sensitivity of the structure increases. If the gold layer is even thicker, the only peak corresponding to the shell is present. Four extinction spectra are presented in Fig. 3 to illustrate their characteristic features in the different shell-size ranges.

The bulk refractive index sensitivities of the core-shell structures with various core and shell thicknesses are plotted in Fig. 4. Simulations were also performed on pure gold nanoparticles resulting in monotonously increasing sensitivity between 50 nm/RIU and 180 nm/RIU for radii between 5 nm and 40 nm, respectively. A similar trend and sensitivity values can be seen in the upper part of Fig. 4 where the dominant peak corresponds to the gold shell. Higher sensitivities than silver spheres of the same size can only be found at the region where the peaks belong to the silver core.

In terms of sensitivity, anomalies can be observed at the transition ranges (marked with empty white squares in Fig. 4), that appear when

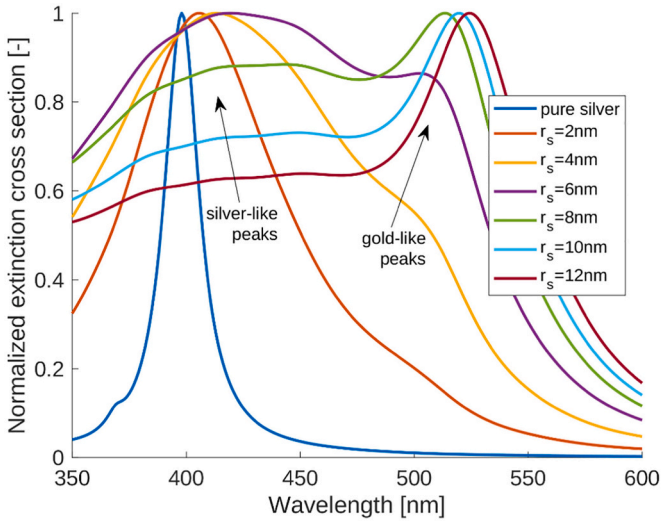

Fig. 3. *Extinction cross-section spectra of $r_c = 22\ nm$ Ag@Au particles with different shell thicknesses at $n = 1.33$.*

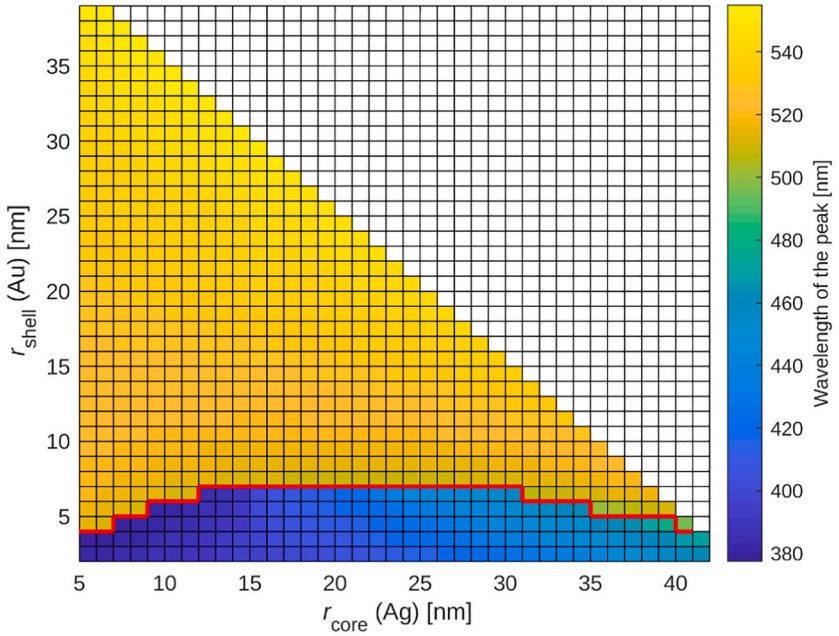

Fig. 2. Position of the highest peak at $n = 1.33$ for Ag@Au core-shell nanoparticles. The red line marks the transition from the silver core to the gold shell. (For interpretation of the references to colour in this figure legend, the reader is referred to the web version of this article.)

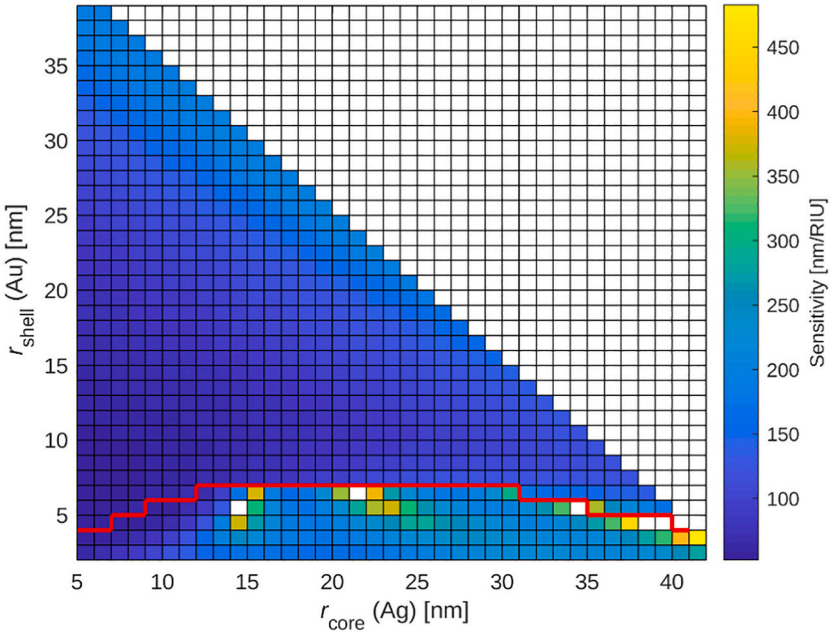

Fig. 4. Bulk refractive index sensitivity chart of Ag@Au core-shell nanostructures. The white squares mark empty data, where the shift of the spectra could not be properly evaluated.

the peaks merge or flatten, often accompanied by the appearance of hybrid peaks. Although these anomalies could appear as a jump-like increase in sensitivity (if evaluated with the same methodology), however, these cases are not suitable for sensors due to the widened peaks and have therefore been cut out of the sensitivity figures.

To demonstrate which core-shell sizes are preferable compared to pure silver, a separate figure has been plotted in Fig. 5. The enhancement shows the sensitivity of a particular core-shell particle divided by the sensitivity of an Ag particle of the same external size: $r_{core} + r_{shell} = r_{cs\ full} = r_{Ag}$.

In Fig. 5 two distinct hot-spot regions with enhanced sensitivities can be observed: one at 14 ± 2 nm core radius with 4 ± 2 nm shell thickness and one at 22 ± 2 nm core radius with 6 ± 1 nm shell thickness. These enhancement hot-spots correspond well with the positions of the highest obtainable sensitivities in Fig. 4. These presence of these hot-spots is due to the merging of the core-shell materials' peaks close to the peak dominance transition threshold (where the dominant peak shifts from the core to the shell material, marked with a red line). This merging naturally comes with increased peak widths, which can be disadvantageous for some practical applications.

In other words, the increased sensitivity comes with a tradeoff of a worse figure of merit (FOM, characterized by the sensitivity/peak full width at half maximum), as can be seen in the presented spectra of Fig. 3. However, most of the area below the transition threshold (red

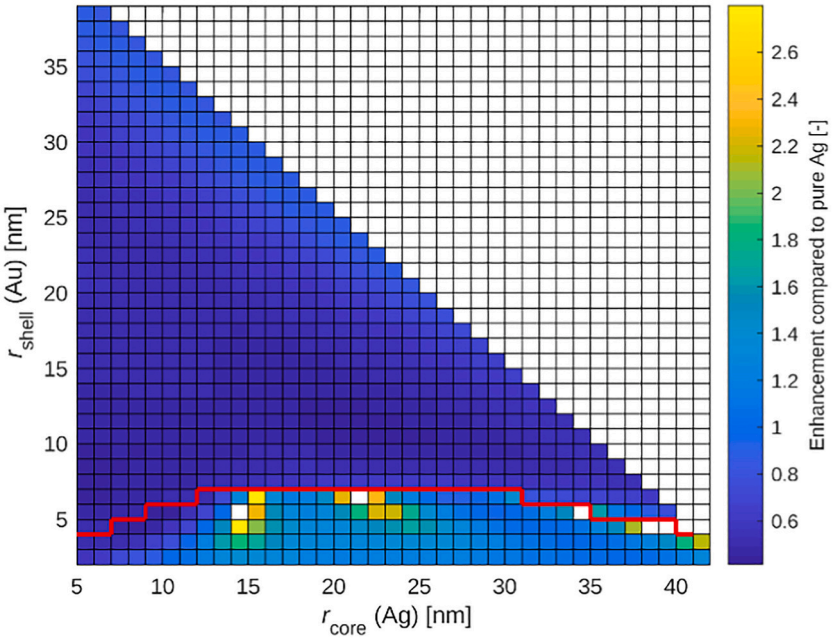

Fig. 5. Sensitivity enhancement of Ag@Au core-shell nanostructures compared to pure Ag nanospheres with the same total size. The white squares mark empty data, where the shift of the spectra could not be properly evaluated.

line, in Figs. 4 and 5) has enhancement above one, so very thin gold shells on silver cores can still be advantageous in terms of sensitivity without significantly reducing the sensor's FOM. Similarly to the previous figure, the calculated FOM was also plotted in Fig. 6. This map confirms that the FOM also has local maxima in the position of sensitivity hot-spots, which consolidates our previous recommendations.

From a practical point of view, another advantage of a thin gold shell is that such core-shell NPs are more stable and resistant to oxidation than pure silver particles. Thus by using a thin gold shell relative to the core's diameter, this advantage can be exploited without significantly affecting the usual properties of the silver core and even enhancing its refractive index sensitivity with a factor of 1.2–2.5, depending on the shell size.

3.2. The sensitivity of Au@Ag core-shell nanostructures

As mentioned before, the extinction cross-section of silver nanoparticles can reach much larger values than gold particles of the same geometry [28]. Based on this, it is not unexpected that applying a thin layer of silver to the gold particles drastically changes the characteristics of the extinction spectrum.

In Fig. 7 characteristic spectra corresponding to various shell thicknesses at a fixed core size are shown, while Fig. 8 presents the positions of the highest peaks for Au@Ag core-shell nanostructures, simulated at $n = 1.33$. Similar to Ag@Au particles, the figure can be divided into two main regions. In the case of relatively thin shells compared to the cores (right side of Fig. 8), particles have a gold-like extinction spectrum. In this range, the wavelengths of the prominent peaks are typically greater than 490 *nm*.

The shape of the boundary separating the two domains (marked with red in Figs. 8 and 9) is different from what we have seen for the Ag@Au case.

The bulk refractive index sensitivities of the different core-shell structures are plotted in Fig. 9. At $r_c \approx 27$ *nm*, the boundary is blurred due to the merged peaks, the transition between the dominant peaks (from gold to silver) is continuous in this region. High sensitivity regions are located along this borderline. The increase in the sensitivity can be associated with the increased dominance of the peaks belonging to the silver shell (at lower wavelengths). Other hot-spot regions can be observed at core radii around 19–22 nm, at shell thicknesses between 9 and 15 nm.

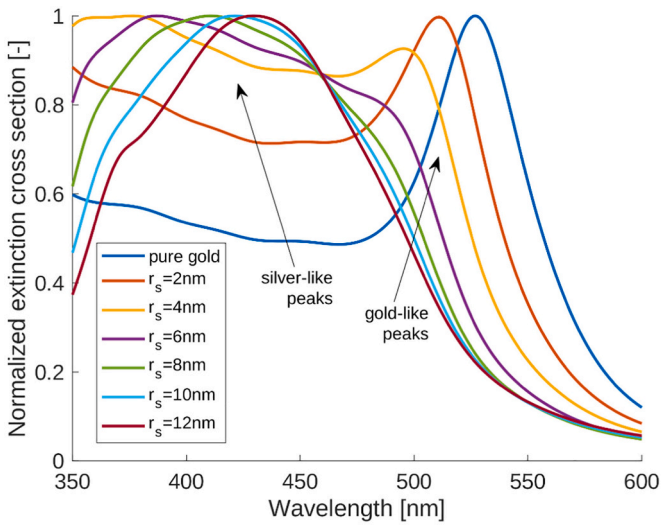

Fig. 7. *Extinction cross-section spectra of $r_c = 22$ nm Au@Ag particles with different shell thicknesses at $n = 1.33$.*

Fig. 10 shows the enhancement values, calculated in comparison with a pure Au nanosphere with similar thickness. For thicker shells (e.g.,>10–15 nm), the extinction spectra and sensitivities are similar to those usual for silver, which accounts for the stable 2–3 enhancement compared to pure gold. In the right side of Fig. 9, the spectra and sensitivities are similar to gold, thus the enhancement is around 1. An optimal region for fabrication could be identified around 20±3 nm core size with 10±3 nm shell thickness, where the enhancement yielded by the silver shell can be 2–5× compared to a pure gold particle. It has to be noted that again, the cost of increased sensitivity is a decrease in the FOM due to increased peak width (see Fig. 11). Here the local maxima in the FOM map also correspond well with the sensitivity hot-spots of Fig. 9, but it has to be noted that the FOM in these local maxima is significantly smaller (e.g. 0.5×), then the FOM corresponding to pure

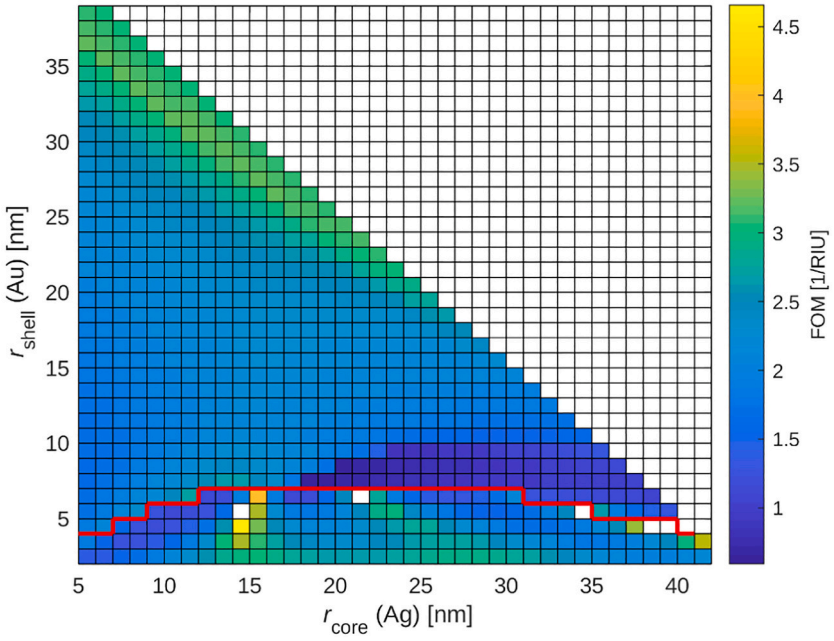

Fig. 6. The figure of merit (FOM) of Ag@Au core-shell nanostructures in the function of core and shell thicknesses. The white squares mark empty data, where the shift of the spectra could not be properly evaluated.

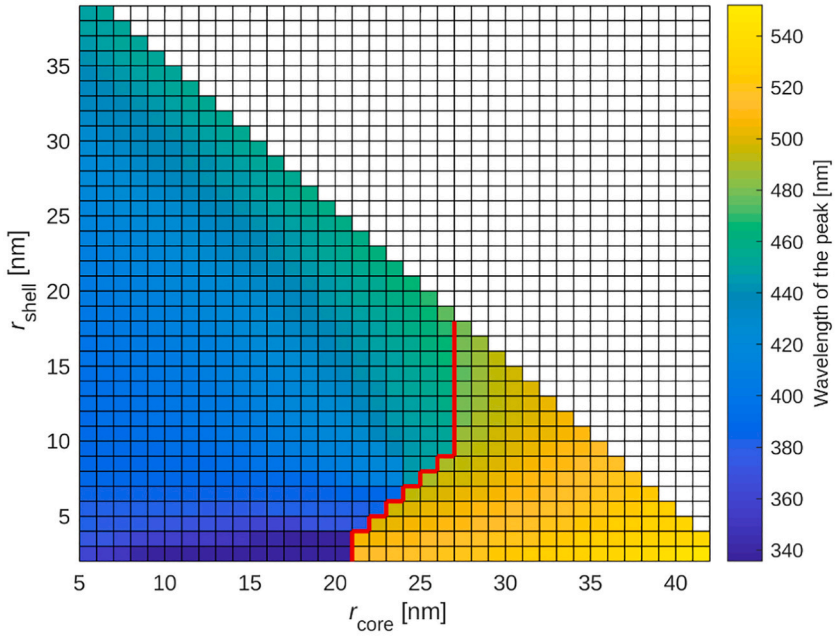

Fig. 8. Position of the highest peak at n = 1.33 for Au@Ag core-shell nanoparticles.

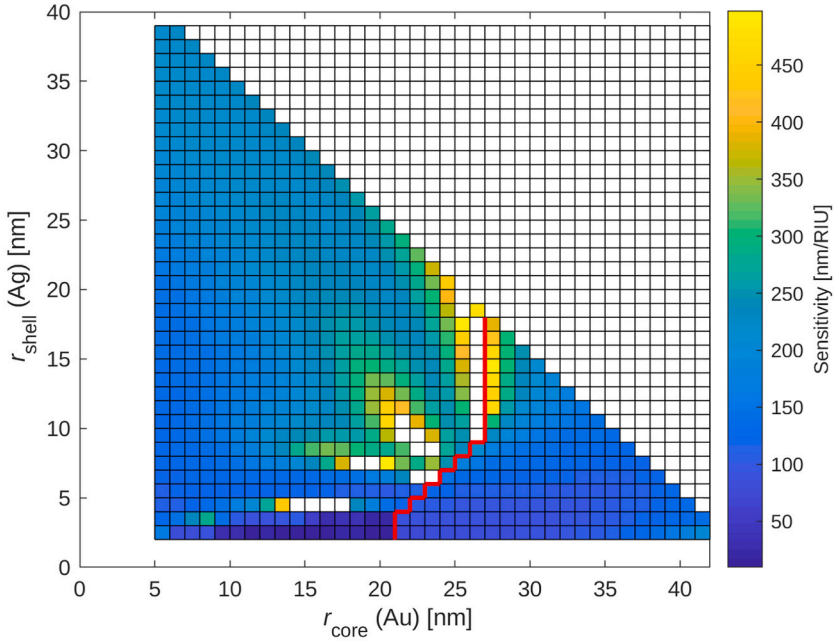

Fig. 9. Bulk refractive index sensitivity chart of Au@Ag core-shell nanostructures. The white squares mark empty data, where the shift of the spectra could not be properly evaluated.

silver (left side of Fig. 11 with small Au core sizes). Also, covering the gold particles with a thin silver layer might not be practical for some sensor applications.

Our results are in good agreement with previously published calculations. The shape of the extinction spectra and the position of the dominant peaks are similar as (radius of the core = r_c, thickness of the shell=r_s): In the case of Ag@Au: ($r_c = 30nm$, $r_s = 2.14nm \approx 2nm$) [34], $r_c = \{10, 20\}nm$, $r_s = \{5, 20\}nm$ [22]. Au@Ag: $r_c = 15nm$, $r_s = (2 \ldots 10)nm$ [35], $r_c = \{10, 20\}nm$, $r_s = \{5, 20\}nm$ [22], $r_c = 13nm$, $r_s = \{2, 4, 9\}nm$ [36]. The latter also contains sensitivity data, which is also consistent with our calculations. (In some articles, the diameter of the particles was used as a parameter, but in the comparison, we used our own convention so the core radii r_c were recorded).

4. Conclusions

By examining Au@Ag and Ag@Au core-shell nanoparticles (with a maximum full radius of 43 nm, minimum core radius and shell thickness of 5 nm and 2 nm, respectively), the dominant absorption peaks (the highest peak of the extinction cross-section spectrum) could be well distinguished based on their origin (silver or gold), only in a few areas are multiple relevant peaks present at once. In the case of Ag@Au, these domains can be sharply separated from each other, while in the Au@Ag system, in a certain range, the dominance changes at the full confluence

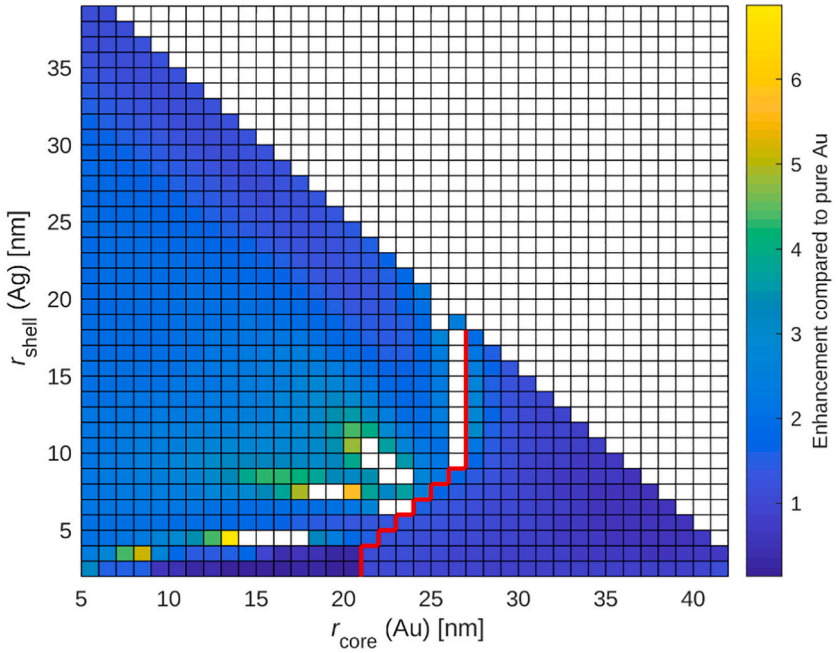

Fig. 10. Sensitivity enhancement of Au@Ag core-shell nanostructures compared to pure Au nanospheres with the same total size. The white squares mark empty data, where the shift of the spectra could not be properly evaluated.

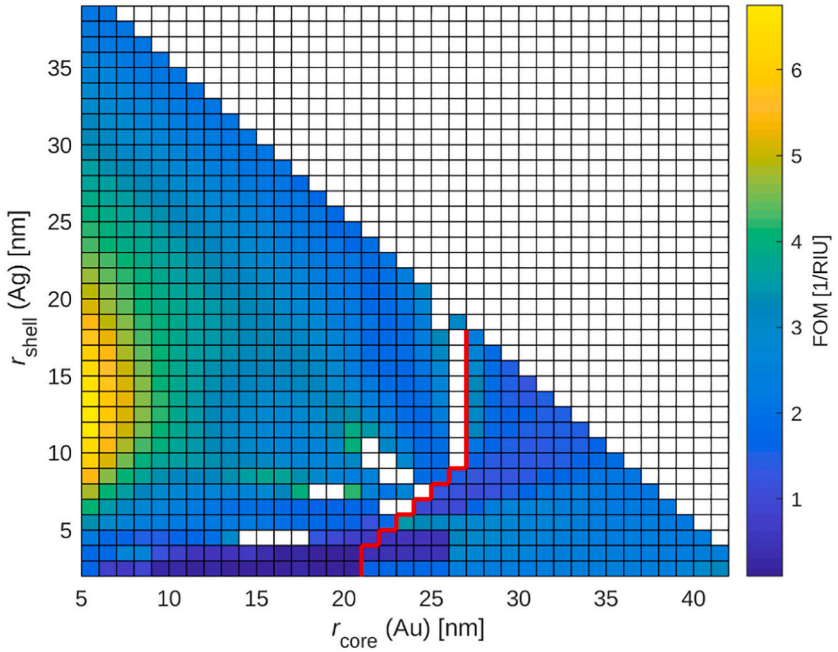

Fig. 11. The figure of merit (FOM) of Au@Ag core-shell nanostructures in the function of core and shell thicknesses. The white squares mark empty data, where the shift of the spectra could not be properly evaluated.

of the peaks. A significant increase in sensitivity compared to single metal particles of the same size can be achieved by using a core-shell structure in the size range dominated by smaller wavelength (silver-derived) peaks. An increase in sensitivity is almost always accompanied by a flattening and widening of a given peak, resulting in reduced FOMs, so finding a compromise is required, considering the given application areas (e.g., type of transducer and signal readout). In terms of sensitivity, Au@Ag structures at the most size range perform better, but from a practical point of view, using Ag@Au systems with a few nm gold shell could a better solution for most applications due to their better chemical stability. The provided sensitivity and figure of merit maps (which are in good correspondence) can be used to optimize the design and fabrication of plasmonic sensors utilizing core-shell nanostructures.

Declaration of Competing Interest

The authors declare that they have no known competing financial interests or personal relationships that could have appeared to influence the work reported in this paper.

Acknowledgments

This research was supported by the EU-funded Hungarian grant EFOP-3.6.2-16-2017-00005. We acknowledge KIFÜ for awarding us access to resource-based in Hungary. This work was supported by the GINOP- 2.3.2-15-2016-00041 Project, which is co-financed by the European Union and the European Regional Development Fund. Istvan Csarnovics is grateful for the support of the János Bolyai Research Scholarship of the Hungarian Academy of Sciences (BO/348/20) and the support through the New National Excellence Program of the Ministry of Human Capacities (ÚNKP-20-5-DE-107).

The research reported in this paper and partially carried out at the Budapest University of Technology and Economics has been supported by the National Research Development and Innovation Fund (TKP2020) based on the charter of bolster issued by the National Research Development and Innovation Office under the auspices of the Ministry for Innovation and Technology.

References

[1] J. Liu, H. He, D. Xiao, S. Yin, W. Ji, S. Jiang, D. Luo, B. Wang, Y. Liu, Recent advances of Plasmonic nanoparticles and their applications, Materials. 11 (2018) 1833, https://doi.org/10.3390/ma11101833.

[2] A. Csáki, O. Stranik, W. Fritzsche, Localized surface plasmon resonance based biosensing, Expert. Rev. Mol. Diagn. 18 (2018) 279–296, https://doi.org/10.1080/14737159.2018.1440208.

[3] A. Bonyár, Label-free nucleic acid biosensing using nanomaterial-based localized surface Plasmon resonance imaging: a review, ACS Appl. Nano Mater. 3 (2020) 8506–8521, https://doi.org/10.1021/acsanm.0c01457.

[4] A. Bonyár, Simulation of the refractive index sensitivity of coupled Plasmonic nanostructures, Proc. Eng. 168 (2016) 962–965, https://doi.org/10.1016/j.proeng.2016.11.316.

[5] E. Hutter, M.-P. Pileni, Detection of DNA hybridization by gold nanoparticle enhanced transmission surface Plasmon resonance spectroscopy, J. Phys. Chem. B 107 (2003) 6497–6499, https://doi.org/10.1021/jp0342834.

[6] S. Kaye, Z. Zeng, M. Sanders, K. Chittur, P.M. Koelle, R. Lindquist, U. Manne, Y. Lin, J. Wei, Label-free detection of DNA hybridization with a compact LSPR-based fiber-optic sensor, Analyst 142 (2017) 1974–1981, https://doi.org/10.1039/C7AN00249A.

[7] L. Soares, A. Csáki, J. Jatschka, W. Fritzsche, O. Flores, R. Franco, E. Pereira, Localized surface plasmon resonance (LSPR) biosensing using gold nanotriangles: detection of DNA hybridization events at room temperature, Analyst 139 (2014) 4964–4973, https://doi.org/10.1039/C4AN00810C.

[8] D. Kawasaki, H. Yamada, K. Maeno, K. Sueyoshi, H. Hisamoto, T. Endo, Core–Shell-structured gold Nanocone Array for label-free DNA sensing, ACS Appl. Nano Mater. 2 (2019) 4983–4990, https://doi.org/10.1021/acsanm.9b00930.

[9] C. Huang, J. Ye, S. Wang, T. Stakenborg, L. Lagae, Gold nanoring as a sensitive plasmonic biosensor for on-chip DNA detection, Appl. Phys. Lett. 100 (2012) 173114, https://doi.org/10.1063/1.4707382.

[10] S. Zhu, H. Li, M. Yang, S.W. Pang, Label-free detection of live cancer cells and DNA hybridization using 3D multilayered plasmonic biosensor, Nanotechnology. 29 (2018) 365503, https://doi.org/10.1088/1361-6528/aac8fb.

[11] T. Lednický, A. Bonyár, Large scale fabrication of ordered gold nanoparticle–epoxy surface Nanocomposites and their application as label-free Plasmonic DNA biosensors, ACS Appl. Mater. Interfaces 12 (2020) 4804–4814, https://doi.org/10.1021/acsami.9b20907.

[12] A. Sakthisabarimoorthi, S.A. Martin Britto Dhas, M. Jose, Preparation of composite Ag@Au core–shell nanoparticles and their linear and nonlinear optical properties, J. Mater. Sci. Mater. Electron. 30 (2019) 1677–1685, https://doi.org/10.1007/s10854-018-0439-5.

[13] A.-M. Hada, M. Potara, S. Suarasan, A. Vulpoi, T. Nagy-Simon, E. Licarete, S. Astilean, Fabrication of gold–silver core–shell nanoparticles for performing as ultrabright SERS-nanotags inside human ovarian cancer cells, Nanotechnology. 30 (2019) 315701, https://doi.org/10.1088/1361-6528/ab1857.

[14] T. Ghodselahi, S. Arsalani, T. Neishaboorynejad, Synthesis and biosensor application of Ag@au bimetallic nanoparticles based on localized surface plasmon resonance, Appl. Surf. Sci. 301 (2014) 230–234, https://doi.org/10.1016/j.apsusc.2014.02.050.

[15] L. Lu, G. Burkey, I. Halaciuga, D.V. Goia, Core–shell gold/silver nanoparticles: synthesis and optical properties, J. Colloid Interface Sci. 392 (2013) 90–95, https://doi.org/10.1016/j.jcis.2012.09.057.

[16] A.K. Samal, L. Polavarapu, S. Rodal-Cedeira, L.M. Liz-Marzán, J. Pérez-Juste, I. Pastoriza-Santos, Size tunable Au@Ag Core–Shell nanoparticles: synthesis and surface-enhanced Raman scattering properties, Langmuir. 29 (2013) 15076–15082, https://doi.org/10.1021/la403707j.

[17] M.P. Navas, R.K. Soni, Laser generated Ag and Ag–au composite nanoparticles for refractive index sensor, Appl. Phys. A. 116 (2014) 879–886, https://doi.org/10.1007/s00339-014-8460-x.

[18] P. Dong, Y. Lin, J. Deng, J. Di, Ultrathin gold-Shell coated silver nanoparticles onto a glass platform for improvement of Plasmonic sensors, ACS Appl. Mater. Interfaces 5 (2013) 2392–2399, https://doi.org/10.1021/am4004254.

[19] J. Deng, J. Du, Y. Wang, Y. Tu, J. Di, Synthesis of ultrathin silver shell on gold core for reducing substrate effect of LSPR sensor, Electrochem. Commun. 13 (2011) 1517–1520, https://doi.org/10.1016/j.elecom.2011.10.010.

[20] M.I. Mishchenko, L.D. Travis, A.A. Lacis, Scattering, Absorption, and Emission of Light by Small Particles, Cambridge University Press, Cambridge; New York, 2002.

[21] E. Prodan, A hybridization model for the Plasmon response of complex nanostructures, Science 302 (2003) 419–422, https://doi.org/10.1126/science.1089171.

[22] V.K. Pustovalov, L.G. Astafyeva, W. Fritzsche, Optical properties of Core–Shell gold–silver and silver–gold nanoparticles for near UV and visible radiation wavelengths, Plasmonics. 7 (2012) 469–474, https://doi.org/10.1007/s11468-012-9330-z.

[23] U. Hohenester, A. Trügler, MNPBEM – a Matlab toolbox for the simulation of plasmonic nanoparticles, Comput. Phys. Commun. 183 (2012) 370–381, https://doi.org/10.1016/j.cpc.2011.09.009.

[24] V. Myroshnychenko, J. Rodríguez-Fernández, I. Pastoriza-Santos, A.M. Funston, C. Novo, P. Mulvaney, L.M. Liz-Marzán, F.J. García de Abajo, Modelling the optical response of gold nanoparticles, Chem. Soc. Rev. 37 (2008) 1792–1805, https://doi.org/10.1039/b711486a.

[25] A. Trügler, Optical Properties of Metallic Nanoparticles 1st ed., 92–95, Springer, 2016, pp. 118–120.

[26] J.D. Jackson, Classical Electrodynamics, 3rd ed, Wiley, New York, 1999, pp. 500–506.

[27] A. Bonyár, G. Szántó, I. Csarnovics, Coupled surface plasmon resonance on gold nanocubes - investigation by simulation, in: 2016 IEEE 22nd International Symposium for Design and Technology in Electronic Packaging (SIITME), IEEE, Oradea, Romania, 2016, pp. 139–141, https://doi.org/10.1109/SIITME.2016.7777263.

[28] J. Singh Sekhon, S., S Verma, refractive index sensitivity analysis of Ag, au, and cu nanoparticles, Plasmonics 6 (2011) 311–317, https://doi.org/10.1007/s11468-011-9206-7.

[29] P.B. Johnson, R.W. Christy, Optical constants of the Noble metals, Phys. Rev. B 6 (1972) 4370–4379, https://doi.org/10.1103/PhysRevB.6.4370.

[30] K.M. Mayer, J.H. Hafner, Localized surface Plasmon resonance sensors, Chem. Rev. 111 (2011) 3828–3857, https://doi.org/10.1021/cr100313v.

[31] G. Qiu, S.P. Ng, C.-M.L. Wu, Bimetallic au-Ag alloy nanoislands for highly sensitive localized surface plasmon resonance biosensing, Sensors Actuators B Chem. 265 (2018) 459–467, https://doi.org/10.1016/j.snb.2018.03.066.

[32] Z. Starowicz, R. Wojnarowska-Nowak, P. Ozga, E.M. Sheregii, The tuning of the plasmon resonance of the metal nanoparticles in terms of the SERS effect, Colloid Polym. Sci. 296 (2018) 1029–1037, https://doi.org/10.1007/s00396-018-4308-9.

[33] Y.-W. Ma, L.-H. Zhang, Z.-W. Wu, M.-F. Yi, J. Zhang, G.-S. Jian, The study of tunable local surface Plasmon resonances on au-Ag and Ag-au Core-Shell alloy nanostructure particles with DDA method, Plasmonics. 10 (2015) 1791–1800, https://doi.org/10.1007/s11468-015-9997-z.

[34] R. Borah, S.W. Verbruggen, Silver–gold bimetallic alloy versus Core–Shell nanoparticles: implications for Plasmonic enhancement and Photothermal applications, J. Phys. Chem. C 124 (2020) 12081–12094, https://doi.org/10.1021/acs.jpcc.0c02630.

[35] Y. Chen, H. Wu, Z. Li, P. Wang, L. Yang, Y. Fang, The study of surface Plasmon in au/Ag Core/Shell compound nanoparticles, Plasmonics. 7 (2012) 509–513, https://doi.org/10.1007/s11468-012-9336-6.

[36] A. Steinbrück, O. Stranik, A. Csaki, W. Fritzsche, Sensoric potential of gold–silver core–shell nanoparticles, Anal. Bioanal. Chem. 401 (2011) 1241–1249, https://doi.org/10.1007/s00216-011-5177-y.